Research Square

Preprints are preliminary reports that have not undergone peer review.
They should not be considered conclusive, used to inform clinical practice,
or referenced by the media as validated information.

Process–Property Relationships and Mechanical Tunability of MEX-Fabricated Polycaprolactone for Bioresorbable Stent Materials

Kuang Yee Ng

kuangyee0706@gmail.com

University Malaysia Perlis: Universiti Malaysia Perlis https://orcid.org/0000-0002-8679-4360

Noorhafiza Muhammad

Siti Noor Fazliah Mohd Noor

Mohd Shuhidan Saleh

Kamalakanta Muduli

Research Article

Keywords: Material extrusion (MEX), Polycaprolactone (PCL), Bioresorbable stents (BRS), Process–property relationships, Mechanical tunability

Posted Date: March 23rd, 2026

DOI: https://doi.org/10.21203/rs.3.rs-9089947/v1

License: This work is licensed under a Creative Commons Attribution 4.0 International License.
Read Full License

Abstract

Material extrusion (MEX) has emerged as a promising method for fabricating bioresorbable stents (BRS); however, a systematic understanding of how process parameters regulate material-level compressive and flexural behaviour of polycaprolactone (PCL) under different loading modes remains limited. In this study, the effects of extrusion temperature (T_E), material deposition speed (v_D) and extrusion multiplier (M_E) on the compressive and flexural responses of MEX-fabricated PCL were investigated using a response surface methodology framework. Distinct parameter sensitivities were observed between loading modes, with M_E identified as the dominant factor governing both strength and modulus through its control of volumetric material delivery and consolidation quality, while T_E and v_D acted as secondary modulators. Regression-based statistical models were developed to capture the nonlinear process–property relationships and were subsequently employed to define compression-focused, flexural-focused and multi-objective optimisation pathways, reflecting the clinically relevant trade-off between radial support and conformability in coronary stent design. Microstructural observations from cross-sectional SEM imaging provided mechanistic support for the parameter-dependent trends by revealing variations in material continuity, void distribution and defect suppression. By isolating material behaviour from geometric effects, this work establishes a tunable, geometry-independent mechanical window for MEX-fabricated PCL, offering a quantitative material baseline to support future design and optimisation of BRS architectures.

1.0 Introduction

Coronary artery disease (CAD) remains one of the leading causes of morbidity worldwide, and vascular stents have become an essential intervention to restore luminal patency [1–3]. Once deployed, a stent must withstand a complex mechanical environment, including continuous radial compression from vascular recoil and pulsatile blood pressure, as well as significant bending deformation during crimping, delivery and navigation through tortuous coronary anatomy [4, 5]. These loading conditions place stringent mechanical requirements on stent materials and structures, necessitating sufficient radial strength to resist collapse while simultaneously providing adequate flexural flexibility to ensure trackability and conformability within curved vessels [6–8]. Achieving an optimal balance between these mechanical demands is fundamental to the performance and long-term reliability of coronary stents.

To meet these demanding mechanical requirements, increasing attention has turned toward bioresorbable materials and advanced fabrication strategies for bioresorbable stents (BRS). Such stents provide temporary mechanical support and gradually degrade over time, thereby mitigating the long-term complications associated with permanent metallic implants [9, 10]. Among existing bioresorbable polymers, polycaprolactone (PCL) stands out as an attractive candidate due to its excellent biocompatibility and biodegradability, favourable flexibility and ductility and history of Food and Drug Administration (FDA) approval for use in implantable medical devices [11–14]. Concurrently, the growing adoption of additive manufacturing has positioned material extrusion (MEX) as a promising technique for producing patient-specific stents, offering precise geometric control and on-demand customisation

[15–17]. However, the mechanical performance of MEX-fabricated components is highly sensitive to process parameters, leading to significant variations in the resulting material behaviour [18]. Accordingly, it is crucial to determine how MEX process parameters affect the inherent mechanical properties of PCL to ensure the mechanical performance of the fabricated stent.

Recent studies have increasingly examined how MEX process parameters influence the mechanical behaviour of PCL-based stent structures, with particular attention to radial and flexural performance—two properties that are fundamental to coronary stent function [6–8]. Guerra and Ciurana [19] investigated the effects of nozzle temperature, flow rate and printing speed by evaluating the recoil ratio of PCL stent samples, showing that flow rate above 100% produced wider struts and hinges that enabled greater radial expansion. Wang et al. [20] adopted a more comprehensive mechanical characterisation approach, including three-point bending, radial compression and expansion tests, to examine how extruder rotational speed alters key geometric features such as connector length and beam width, ultimately demonstrating that higher extrusion speeds increase strut width, thereby improving radial strength while reducing bending flexibility. Singh et al. [21] employed a response surface methodology (RSM) to systematically study the influence of layer thickness (t_L) and printing speed on the bending and compression behaviour of solvent-cast PCL-based composite stents, identifying parameter combinations that reduce dimensional shrinkage and enhance overall mechanical stability. Similarly, Kandi and Pandey [22] evaluated tubular PCL-based scaffolds under varying infill density, t_L and print speed, showing that increased infill improves radial load capacity and ductility, whereas faster speed and thicker t_L reduce mechanical performance; their optimisation study further established a parameter set that maximises radial compression load. Collectively, these findings demonstrate that MEX parameters exert clear and measurable effects on the mechanical behaviour of fabricated PCL-based stent structures.

However, meaningful comparison across existing studies remains challenging as their experimental methodologies and sample structures differ substantially. Although prior work consistently shows that radial and flexural behaviours can be modulated through MEX parameters, the mechanical testing protocols used in these studies vary widely, making their findings difficult to reconcile. For instance, Guerra and Ciurana [19] quantified radial performance by expanding samples to their maximum dilation, whereas Wang et al. [20] evaluated recoil only at fixed expansion levels of 10% and 20%, resulting in fundamentally non-comparable measurements. Likewise, the radial compression tests conducted by Kandi and Pandey [22] and by Singh et al. [21] used different compression ranges and loading conditions, raising uncertainty as to whether discrepancies in their reported optimal parameters reflect true processing effects or merely differences in testing procedures. Such inconsistencies underscore the need for more uniform and standardised mechanical evaluation methods.

Beyond differences in testing methodology, the stent geometries employed across these studies also vary considerably, introducing an additional layer of complexity [23]. Each investigation utilised distinct structural patterns, connector or strut dimensions—factors that may exert dominant effects on mechanical performance. In this context, computational and experimental studies in stent mechanics

consistently demonstrate that variations in cell topology, strut geometry, or connector architecture can lead to fundamentally different radial strength, bending flexibility and optimal design strategies [24–28]. Recent review articles further emphasise that stent performance is highly geometry-dependent, such that even small structural modifications can shift the balance between radial support and flexibility, ultimately requiring different optimisation routes for different designs [5, 29, 30]. Under these circumstances, it becomes exceedingly difficult to determine whether the “optimal” process parameters reported in previous studies are genuinely material- or process-driven, or whether they are simply a consequence of the specific stent architectures being tested.

Together, these methodological and geometric inconsistencies highlight a critical gap in current research: the field lacks a geometry-independent, standardised framework for understanding how MEX process parameters influence the intrinsic mechanical response of PCL for coronary stent applications. This motivates the need to decouple material–process effects from sample structural effects, thereby enabling a more controlled and generalisable investigation. Efforts to clarify these parameter–property relationships using a more standardised approach have been limited, particularly for PCL. A few studies have characterised the compressive or flexural behaviour of PCL using standardised mechanical tests or ASTM-inspired specimen geometries, including selective laser sintering (SLS) scaffolds [31, 32] and PCL–cellulose structures [33]. These works provide useful baseline measurements of PCL mechanical behaviour. However, most of these studies did not involve the MEX process, nor did they discuss it in the context of the demand for coronary stents. Moreover, they do not investigate how process parameters systematically influence the intrinsic mechanical response of PCL. In contrast, standard-based and DOE-driven analyses of MEX process parameters are well established for other polymers such as polylactic acid (PLA) [34–37] and polyethylene terephthalate glycol (PETG) [35, 38], yet corresponding studies for PCL, particularly those linking parameter effects to stent-relevant compressive and flexural properties, remain notably scarce.

This gap is especially important as radial strength and flexural flexibility constitute an inherent mechanical trade-off in stent design [5, 20, 39], and different clinical scenarios prioritise these properties differently [40, 41]. A reliable, geometry-independent mechanical characterisation of MEX-fabricated PCL is therefore essential as a foundational input for future structure-level optimisation and patient-specific stent development. Accordingly, there is a clear need for studies that employ standardised specimen designs, controlled MEX parameter schemes and systematic analytical frameworks to isolate and quantify the material–process relationships of PCL. Therefore, this study aims to establish a geometry-independent mechanical characterisation of MEX-fabricated PCL by using ASTM-standard compression (D695) and flexural (D790) specimens to eliminate the influence of stent geometry. A central composite design (CCD) based on RSM is implemented to systematically evaluate the effects of T_E, v_D and M_E on the compressive and flexural strength and modulus of PCL. By developing statistically validated response models and identifying parameter conditions that optimise radial- and flexural-analogous behaviours, this work provides a fundamental material-level framework that can serve as a transferable input for future stent-structure optimisation and patient-specific device design.

2.0 Materials and Methods

2.1 Materials and MEX Fabrication

PCL filament (Fabbxible Technology) with a diameter of 1.75 mm was used for specimen fabrication. All specimens were produced using a MEX system (Artillery® Genius Pro) equipped with a 0.4 mm extrusion nozzle. Specimen designs were created in CAD software (SolidWorks 2022®) and exported in .stl format for slicing (Ultimaker Cura, version 5.2.2). Three key MEX parameters (T_E, v_D and M_E) were selected as the experimental factors, and the ranges of these parameters used in this study (Table 1) were defined based on a combination of reported values in the literature [19–22] and preliminary processability trials. This broad parameter space was intentionally adopted to encompass the full span of processing conditions previously employed for MEX-fabricated PCL stents, thereby enabling as comprehensive and systematic an identification as possible of the dominant process–property relationships and facilitating the reconciliation of inconsistencies among prior studies. The other process parameters were maintained at the slicing software default settings. No additional post-processing was performed on the specimens after fabrication, in order to preserve the as-fabricated microstructural features induced by the selected process parameters and to isolate their intrinsic effects on mechanical behaviour. This approach enables direct attribution of the measured mechanical responses to variations in MEX processing conditions rather than to secondary surface modification steps.

Table 1
The levels of the three key MEX parameters studied.

Process Parameter	T_E (℃)	v_D (mm/s)	M_E (%)
Low Level	80	5	70
High Level	250	50	150

2.2 Specimen Preparation

Two types of standardised solid specimens were prepared in compliance with ASTM D695 and ASTM D790 for compression and flexural testing, respectively. The compression specimens were cylindrical (12.7 mm in diameter and 25.4 mm in height), while the flexural specimens were rectangular bars (127 mm × 12.7 mm × 3.2 mm). To eliminate geometric influences and focus solely on the effects of process parameters, standardised solid specimens were employed in this study instead of the stent-like geometries used previously.

2.3 Experimental Design

To systematically evaluate the effects of the selected parameters, a statistical design of experiments approach was adopted. A CCD within the framework of RSM was employed to investigate the combined effects of T_E, v_D and M_E. A face-centred CCD ($\alpha = 1$) was selected to maintain all factor levels within the

feasible operating range, resulting in a total of 17 experimental runs, with three centre-point runs included to monitor experimental stability. Five replicates (n = 5) were produced and examined for each parameter combination.

2.4 Mechanical Testing

Mechanical testing was conducted to evaluate the compressive and flexural performance of the fabricated PCL specimens. All tests were performed using a computer-controlled electronic universal testing machine (Shimadzu AGS-X) under ambient laboratory conditions (25°C).

Compression testing followed the procedures of ASTM D695, using the cylindrical specimens described in Section 2.2. The samples were compressed between two parallel plates at a crosshead speed of 1.0 mm/min using a 50 kN load cell, and the test was terminated once 50% strain was reached. The compressive modulus was determined from the initial linear region (3–6% strain). As slight variations in the final termination strain occurred when applying the nominal 50% strain limit to as-fabricated specimens, the stress value at 49.5% strain was used as a consistent reference for compressive strength evaluation across all parameter conditions.

Flexural testing was conducted in accordance with ASTM D790, using the rectangular specimens specified in Section 2.2. Tests were performed in a three-point bending configuration with a support span of 51.2 mm at a crosshead speed of 1.3 mm/min using a 50 kN load cell. The tests were terminated at 5% strain. The flexural modulus was determined from the initial linear region (1–4% strain). Similarly, flexural strength was reported at 4.5% strain to ensure consistent data extraction prior to the strain-controlled termination limit, enabling unbiased comparison across the investigated parameter conditions.

2.5 Microstructural Characterisation

Microstructural analysis was performed to examine how MEX process parameters influence the internal morphology of the fabricated PCL specimens. Dedicated specimens were sectioned to expose their cross-sectional surfaces, which were then sputter-coated with a thin layer of platinum using an ion sputter coater (COXEM SPT-20). The coated surfaces were imaged using a tabletop scanning electron microscope (Hitachi TM3000) at an accelerating voltage of 10 kV and a magnification of 100×. The SEM images were used to assess interlayer bonding quality and the presence of internal voids or porosity associated with different processing conditions, as these microstructural features are known to play a critical role in the resulting compressive and flexural behaviour.

2.6 Data Analysis and Optimisation

Statistical analyses were performed using statistical software (Minitab®, version 21.4) based on RSM. A second-order (quadratic) regression model was fitted to describe the relationships between T_E, v_D and M_E with the compressive and flexural responses. The model significance was evaluated through ANOVA ($p < 0.05$). Single- and multi-response optimisation was conducted using the desirability function approach to maximise the compressive- and flexural-related properties.

3.0 Results and Discussion

3.1 Mechanical Behaviour under Compression and Flexure

In the present study, T_E, v_D and M_E were selected as the process parameters of interest, as they are widely recognised as the primary MEX variables dominating the effective mechanical response of fabricated parts in the context of PCL-based BRS fabrication [19–22]. Meanwhile, compressive and flexural strength and modulus were adopted as the mechanical evaluation metrics, as they capture the fundamental material responses that govern radial support and deformation resistance in coronary stent applications. Strength reflects the load-bearing capacity before failure, while modulus reflects the stiffness that resists radial and bending deformation—both of which directly underpin a stent's ability to maintain lumen patency. Although the loading configurations differ, radial and flexural behaviour is fundamentally governed by the intrinsic elastic modulus and strength of the material [24, 42, 43]. Accordingly, optimising these key parameters offers a direct means to enhance the radial- and flexural-load-bearing capability of fabricated PCL at the material level, complementing geometry-based strategies commonly used to improve stent mechanical performance. Based on this framework, a CCD-based RSM was implemented to systematically explore the effects of T_E, v_D and M_E on the compressive and flexural behaviour of MEX-fabricated PCL specimens. The resulting stress–strain responses obtained from ASTM-standard compression and flexural tests are presented in Fig. 1. Table 2 summarises the complete CCD matrix, together with the corresponding experimentally measured strength and modulus values extracted from the stress–strain curves.

Table 2
CCD of RSM used in the DOE. Results of strength and modulus obtained from the PCL compressive and flexural tests are shown.

Set	Process Parameters			Compressive Response		Flexural Response	
	T_E (℃)	v_D (mm/s)	M_E (%)	Strength (MPa)	Modulus (MPa)	Strength (MPa)	Modulus (MPa)
1	80	5	70	7.37 ± 1.12	73.39 ± 3.85	7.53 ± 0.52	180.63 ± 11.81
2	250	5	70	7.02 ± 0.95	51.90 ± 9.91	5.67 ± 1.65	133.52 ± 41.67
3	80	50	70	7.48 ± 0.79	60.60 ± 5.84	7.42 ± 0.45	176.00 ± 11.97
4	250	50	70	8.28 ± 0.62	69.02 ± 13.28	4.84 ± 0.49	113.67 ± 11.22
5	80	5	150	29.27 ± 1.65	227.43 ± 14.64	7.50 ± 0.57	175.62 ± 13.65
6	250	5	150	36.38 ± 1.02	233.79 ± 13.49	14.80 ± 0.83	353.78 ± 20.09
7	80	50	150	29.95 ± 1.27	241.78 ± 28.24	12.50 ± 5.30	288.01 ± 128.59
8	250	50	150	39.82 ± 0.44	276.33 ± 21.48	15.67 ± 0.82	375.15 ± 19.74
9	80	27.5	110	25.60 ± 1.36	229.71 ± 13.49	18.05 ± 1.02	431.08 ± 21.82
10	250	27.5	110	27.25 ± 0.95	201.67 ± 8.20	14.80 ± 0.59	351.11 ± 9.75
11	165	5	110	26.28 ± 1.23	209.68 ± 13.08	15.65 ± 0.78	367.96 ± 19.90
12	165	50	110	27.77 ± 0.75	206.70 ± 7.77	15.22 ± 0.39	358.91 ± 10.88
13	165	27.5	70	9.40 ± 0.38	78.67 ± 4.18	6.70 ± 0.83	155.10 ± 21.02
14	165	27.5	150	35.75 ± 0.40	273.67 ± 11.73	17.35 ± 2.39	406.22 ± 58.31
15	165	27.5	110	28.35 ± 0.24	185.20 ± 16.61	18.47 ± 0.48	434.26 ± 11.75
16	165	27.5	110	28.89 ± 0.21	219.62 ± 11.51	17.60 ± 0.59	418.32 ± 15.58

Set	Process Parameters			Compressive Response		Flexural Response	
	T_E (℃)	v_D (mm/s)	M_E (%)	Strength (MPa)	Modulus (MPa)	Strength (MPa)	Modulus (MPa)
17	165	27.5	110	28.48 ± 0.35	199.05 ± 13.93	16.48 ± 0.45	387.87 ± 11.91

(a) Effects of Extrusion Temperature

Figure 2 presents the main effects of T_E, v_D and M_E on the compressive and flexural strength and modulus of the fabricated PCL specimens. With respect to T_E, T_E generally enhances both compressive and flexural strength, although the responses are non-monotonic across the investigated range. Strength values increase with T_E up to an intermediate optimum before slightly declining at higher T_E, whereas the elastic modulus exhibits only minor variation, indicating a comparatively weak sensitivity to thermal input.

Despite the presence of non-linear trends, the overall influence of T_E across the full range from 80 to 250°C remains moderate, with compressive and flexural strength increasing by approximately 15.38% and 3.43%, respectively, while changes in compressive and flexural modulus are limited (0.018% and 3.93%, respectively). These results suggest that T_E primarily influences failure-related strength, particularly under compression, rather than elastic response, while further increases in T_E beyond an intermediate level provide limited additional benefit.

This behaviour is consistent with the thermorheological characteristics of semi-crystalline polymers such as PCL. Increasing T_E typically improves melt fluidity and interlayer fusion, promoting more effective load transfer under mechanical loading, whereas excessive thermal input may offset these benefits through material degradation or geometric instability. Similar temperature-dependent strengthening trends have been widely reported for MEX-fabricated thermoplastics including PLA, PETG and high-performance polymers such as polyetheretherketone (PEEK), where enhanced melt mobility and reduced interlayer separation lead to improved mechanical integrity [38, 44, 45]. The present results confirm that this general mechanism also applies to PCL, whose low melting temperature and high viscosity sensitivity render its mechanical performance particularly responsive to thermal conditions during deposition.

(b) Effects of Material Deposition Speed

Figure 2 also illustrates the main effects of v_D on the compressive and flexural strength and modulus of the fabricated PCL specimens. In contrast to T_E, the influence of v_D on all four mechanical responses is comparatively moderate and exhibits a shallow non-monotonic trend across the investigated range.

As v_D increases from 5 mm/s, both compressive and flexural strength gradually increase, reaching maximum values at intermediate speeds (≈ 30–35 mm/s), before showing a slight decline at higher v_D. A similar response is observed for the corresponding moduli, with only limited variation across the full range. When comparing the extreme conditions, increasing v_D from 5 to 50 mm/s results in modest net changes of approximately 5–6% for both the compressive and flexural strength and modulus, indicating that v_D exerts a secondary influence on mechanical performance relative to other process parameters.

The presence of an intermediate optimal v_D suggests a balance between deposition continuity and thermal–temporal interaction during extrusion. At low v_D, prolonged residence time may promote thermal dissipation and material over-softening, while at excessively high v_D, insufficient inter-path contact time may limit interlayer consolidation. The relatively flat response profiles observed here indicate that PCL exhibits a broad processing window with respect to v_D, within which mechanical properties remain comparatively stable.

Although prior studies on materials such as PLA, PETG and PEEK frequently report monotonic reductions in strength with increasing v_D [37, 38, 45], the present results highlight that the rate sensitivity of PCL is less pronounced. This discrepancy is likely associated with the low melting temperature and high thermal diffusivity of PCL, which mitigate the adverse effects of reduced deposition time at elevated v_D.

(c) Effects of Extrusion Multiplier

Figure 2 further illustrates the main effects of M_E on the compressive and flexural strength and modulus of the fabricated PCL specimens. Among the investigated process parameters, M_E exerts the most pronounced influence on all four mechanical responses, with substantially larger variations observed across the studied range compared with T_E and v_D.

As M_E increases, compressive strength and modulus increase monotonically, indicating a strong sensitivity of compressive load-bearing capacity to deposited material volume. In contrast, the flexural responses exhibit a non-monotonic dependence on M_E, increasing up to an intermediate optimum before declining at higher M_E.

When evaluated across the full M_E range from 70% to 150%, the overall changes are substantial, with compressive strength and modulus increasing by approximately 271% and 239%, respectively, while flexural strength and modulus increase by approximately 83% and 84%. These magnitudes are markedly larger than those associated with T_E and v_D, confirming that M_E is the dominant parameter governing the mechanical behaviour of MEX-fabricated PCL within the investigated design space.

The pronounced sensitivity to M_E underscores the importance of deposited material volume in governing internal porosity, inter-bead contact and effective load-bearing cross-sectional area. Although direct

investigations of M_E in MEX are limited, similar mechanisms have been widely discussed in studies on infill density, where increased material content reduces void fraction and enhances stress-transfer continuity [37, 38, 46, 47]. In this context, the present findings suggest that M_E serves as an effective process-level control of material volume, while excessive flow may compromise geometric fidelity and bending stress distribution, leading to reduced flexural performance at high M_E.

(d) Statistical Significance and Relative Influence of Process Parameters

The statistical significance and relative influence of T_E, v_D and M_E were evaluated using ANOVA based on the developed response surface models. Separate analyses were conducted for compressive strength, compressive modulus, flexural strength and flexural modulus, and the key statistical metrics are summarised in Table 3.

For the compressive responses, M_E is identified as the overwhelmingly dominant parameter. In the case of compressive strength, M_E exhibits an exceptionally high F-value (8760.63, $p < 0.001$) and accounts for 97.67% of the total contribution among the main factors, whereas T_E and v_D contribute only marginally (2.05% and 0.28%, respectively), despite both being statistically significant ($p < 0.001$). A similar trend is observed for compressive modulus, where M_E remains the sole statistically significant parameter ($p < 0.001$) and contributes 99.60% of the total variation, while the effects of T_E and v_D are negligible.

A comparable dominance of M_E is also evident in the flexural responses. For flexural strength, M_E shows the highest F-value (170.10, $p < 0.001$) and contributes 97.84% of the total variation, whereas neither T_E nor v_D reaches statistical significance ($p > 0.05$). Likewise, for flexural modulus, M_E again governs the response, contributing 97.81% with a statistically significant effect ($p < 0.001$), while the contributions of T_E and v_D remain minor and statistically insignificant. These statistical trends are consistent with the main effect plots in Fig. 2, where variations in M_E induce substantially larger response amplitudes than those associated with T_E and v_D across all mechanical metrics.

Thus, the ANOVA results demonstrate that, within the investigated design space, the mechanical behaviour of MEX-fabricated PCL is predominantly governed by M_E, irrespective of the loading mode. In contrast, T_E and v_D play secondary roles, with limited contributions and inconsistent statistical significance across responses. This finding highlights the critical importance of volumetric material deposition in controlling load-bearing capacity and elastic modulus, and motivates a microstructural examination of how variations in M_E influence void distribution, filament bonding and interlayer morphology.

Table 3
ANOVA results showing F-values, *p*-values and percentage contribution of T_E, v_D and M_E to compressive strength, compressive modulus, flexural strength and flexural modulus based on the response surface models.

Response	Factor	F-value	p-value	Contribution (%)
Compressive strength	T_E	184.22	0.000	2.05
	v_D	24.74	0.000	0.28
	M_E	8760.63	0.000	97.67
Compressive modulus	T_E	0.00	0.993	0.00
	v_D	6.48	0.013	0.40
	M_E	1614.47	0.000	99.60
Flexural strength	T_E	1.04	0.311	0.60
	v_D	2.72	0.103	1.57
	M_E	170.1	0.000	97.84
Flexural modulus	T_E	1.31	0.255	0.80
	v_D	2.29	0.134	1.39
	M_E	160.97	0.000	97.81

3.2 Microstructural Evidence and Mechanistic Interpretation

Cross-sectional SEM imaging at 100× magnification was employed to qualitatively assess consolidation-related morphological features associated with the parameter-dependent mechanical responses discussed in Section 3.1. At this magnification, the analysis focuses on material continuity, underfilled regions, void-like features and inter-layer consolidation, rather than fine-scale fracture mechanisms. Extreme parameter levels (low and high T_E, v_D and M_E) were selected to maximise observable morphological contrast and to elucidate the dominant mechanisms governing mechanical performance in MEX-fabricated PCL.

For T_E, specimens fabricated at low T_E (80°C) and high T_E (250°C) exhibit broadly similar macroscopic surface morphologies, characterised by relatively smooth cross-sections with limited large-scale voids (Fig. 3a, b and Fig. 4a, b). However, low-T_E samples occasionally display subtle discontinuities and less uniform material regions, consistent with restricted melt mobility and reduced inter-road fusion. In

contrast, high-T_E samples show more continuous and homogeneous cross-sections, indicative of improved melt flow and consolidation. The modest nature of these morphological differences aligns with the comparatively weak sensitivity of elastic modulus to T_E and the non-monotonic strength trends observed in Section 3.1.

Variations in v_D similarly produce only subtle changes in cross-sectional morphology at the examined scale (Fig. 3c, d and Fig. 4c, d). Low-v_D specimens exhibit relatively uniform material distribution, while high-v_D conditions show slightly increased surface irregularity, reflecting reduced interaction time between deposited filaments. The absence of pronounced microstructural disruption supports the statistical findings that v_D exerts a secondary influence on both compressive and flexural responses within the investigated range.

In contrast, changes in M_E give rise to pronounced and readily observable morphological differences. Low-M_E specimens (70%) display clear underfilled regions, sparse material packing and prominent void-like features within the cross-section (Fig. 3e and Fig. 4e), indicative of insufficient volumetric material delivery. Conversely, high-M_E specimens (150%) exhibit dense, continuous material regions with markedly reduced defect prevalence (Fig. 3f and Fig. 4f). These consolidation-related differences directly support the strong and dominant influence of M_E on both strength and modulus identified in the ANOVA and main effect analyses.

Taken together, the SEM observations provide a coherent microstructural basis for the statistical significance trends reported in Section 3.1. While T_E and v_D primarily modulate melt mobility and deposition stability with relatively subtle morphological manifestations, M_E governs volumetric packing efficiency and defect suppression, emerging as the principal determinant of mechanical integrity in MEX-fabricated PCL. The convergence of morphological and statistical evidence confirms that consolidation quality, controlled predominantly by material flow rate, underpins the observed mechanical behaviour.

3.3 Statistical Modelling, Optimisation and Relevance to Stent Design

Building on the mechanistic insights established in Sections 3.1 and 3.2, this section translates the identified parameter–microstructure–mechanics relationships into quantitative predictive models and clinically relevant optimisation frameworks. Due to the fact that clinical implantation does not require a single mechanical profile, but rather a context-dependent balance between radial strength and flexural compliance, three optimisation pathways were defined in this study: (1) A compression-focused optimisation prioritises maximal compressive strength and modulus to represent scenarios where enhanced radial support is required. (2) A flexural-focused optimisation targets high flexural strength while minimising flexural modulus, corresponding to applications demanding improved conformability and resistance to fracture under bending. (3) In addition, a multi-objective optimisation was implemented to balance all four mechanical responses simultaneously, explicitly capturing the trade-off between radial rigidity and vascular compliance that underpins contemporary stent design.

Regression models obtained from RSM (**Eqs. 1–4**) were used to generate predictive relationships between T_E, v_D and M_E and the resulting mechanical responses. Table 4 summarises the optimised parameter sets obtained under different optimisation strategies. Although the optimised points coincided with previously tested design points, their corresponding experimental responses were used to validate the model predictions. The small prediction errors observed across all responses confirm that the regression models provide reliable estimates of PCL mechanical behaviour within the investigated parameter space.

Compressive strength (MPa)	**=**	**$-47.14 + 0.0190\ T_E + 0.0495\ v_D + 0.9597\ M_E - 0.000213\ T_E{*}T_E - 0.001866\ v_D{*}v_D - 0.003370\ M_E{*}M_E + 0.000255\ T_E{*}v_D + 0.000608\ T_E{*}M_E + 0.000383\ v_D{*}M_E$**	**(1)**
Compressive modulus (MPa)	=	$-286.1 - 0.323\ T_E - 0.356\ v_D + 7.204\ M_E + 0.000000\ T_E{*}T_E - 0.01481\ v_D{*}v_D - 0.02470\ M_E{*}M_E + 0.00380\ T_E{*}v_D + 0.001984\ T_E{*}M_E + 0.00730\ v_D{*}M_E$	(2)
Flexural strength (MPa)	=	$-28.14 - 0.0083\ T_E + 0.1717\ v_D + 0.6987\ M_E - 0.000121\ T_E{*}T_E - 0.00369\ v_D{*}v_D - 0.003300\ M_E{*}M_E - 0.000317\ T_E{*}v_D + 0.000549\ T_E{*}M_E + 0.000944\ v_D{*}M_E$	(3)
Flexural modulus (MPa)	=	$-656 - 0.461\ T_E + 4.02\ v_D + 16.74\ M_E - 0.00235\ T_E{*}T_E - 0.0881\ v_D{*}v_D - 0.07962\ M_E{*}M_E - 0.00694\ T_E{*}v_D + 0.01378\ T_E{*}M_E + 0.02198\ v_D{*}M_E$	(4)

Table 4 Optimised MEX process parameter sets obtained under different optimisation strategies, together with RSM-predicted values, experimentally measured responses and corresponding prediction errors for compressive and flexural properties of PCL.

No.*	T_E (°C)	v_D (mm/s)	M_E (%)	Optimisation results			
				Optimised responses*	Predicted value (MPa)	Actual value (MPa)	Error (%)
1	250	50	150	σ_C	39.062	39.82 ± 0.44	1.90
				E_C	279.81	276.33 ± 21.48	1.26
2	80	50	150	σ_F	12.712	12.50 ± 5.30	1.70
				E_F	294.5	288.01 ± 128.59	2.25
3	250	50	150	σ_C	39.062	39.82 ± 0.44	1.90
				E_C	279.81	276.33 ± 21.48	1.26
				σ_F	15.787	15.67 ± 0.82	0.75
				E_F	376.8	375.15 ± 19.74	0.44

*No. indicate the optimisation strategies: 1 is compression-focused, 2 is flexural-focused and 3 is a multi-objective optimisation strategy.

*σ_C refers to compressive strength, E_C refers to compressive modulus, σ_F refers to flexural strength, E_F refers to flexural modulus.

It should be emphasised that the optimised parameter sets identified in this study represent material-level extrema within the investigated design space rather than directly applicable processing conditions for stent fabrication. In particular, although a high M_E (150%) maximises compressive and flexural performance by enhancing volumetric material delivery and consolidation, such conditions are expected to compromise dimensional fidelity and surface quality, especially for fine stent struts. Similarly, despite the ability to fabricate specimens at elevated T_E (250°C) with enhanced strength, the observed non-monotonic dependence of mechanical responses on T_E suggests that excessive thermal input may offset consolidation benefits through degradation or geometric instability. Accordingly, the present optimisation defines an upper bound of achievable material-level mechanical performance under MEX processing, while future multi-objective optimisation should integrate mechanical, morphological and biological performance requirements to identify clinically viable processing windows.

To contextualise the optimised mechanical responses, the results were compared against reported ranges for solid PCL specimens fabricated using different manufacturing methods and tested under

standardised compression or flexural configurations. Published compressive moduli for bulk PCL typically fall within the range of 300–325 MPa, with compressive strengths reported in the range of 34–39 MPa for injection-moulded and SLS-fabricated specimens [31, 32, 48]. The compression-optimised condition identified in the present study yields compressive modulus and strength values approaching the upper region of these reported ranges. A similarly broad distribution is evident in reported flexural properties of PCL, with flexural strength values spanning approximately 11–24 MPa and flexural moduli ranging from 109 to 423 MPa, largely depending on manufacturing process, molecular weight and porosity [49–53]. The flexural-optimised condition obtained in this work likewise falls well within the broad envelope defined by existing PCL reports.

Considering that alternative manufacturing routes, such as SLS and injection moulding, generally produce highly consolidated structures with minimal void content, the ability of MEX-fabricated PCL to attain comparable modulus and strength after parameter optimisation underscores the substantial influence of extrusion-based processing conditions on material consolidation and load transfer. As the compressive and flexural strength in this study were evaluated at strain levels of 49.5% and 4.5%, respectively (as defined in Section 2.4), comparisons with literature values reported at nominally 50% (compression) and 5% (flexure) strain are intended to indicate general trends and ranges rather than exact numerical equivalence. Notably, the multi-objective condition also achieved a balanced mechanical response across both compressive and flexural loading, indicating that the mechanical behaviour of MEX-fabricated PCL can be systematically tuned through process-parameter selection rather than being confined to a narrow range associated with default fabrication settings.

Although stent-level radial and flexural performance arise from the combined contributions of material properties and geometric design [28], the present study intentionally isolates the material component by characterising PCL under standardised ASTM compression and flexural testing. By excluding geometry-dependent effects such as strut thickness, cell topology and hinge mechanics, this approach provides a generalisable assessment of how MEX process parameters regulate the intrinsic modulus and strength of the polymer itself. These material-level properties correspond to the modulus-dependent term in stent mechanical descriptors such as radial stiffness and bending compliance [54], and therefore define the baseline upon which any specific stent geometry must operate.

When viewed within this material-centric framework, the optimised PCL responses can be positioned relative to established BRS backbone materials. Commercial BRS platforms such as Absorb, DESolve and MeRes100 predominantly employ poly(L-lactic acid) (PLLA), which typically exhibits moduli on the order of 2–4 GPa and strengths of 50–70 MPa [42, 55, 56]. While these values reflect bulk material properties rather than assembled stent performance, they define a widely accepted strength and modulus hierarchy for stent backbones. The optimised PCL obtained in the present study exhibits compressive and flexural moduli in the sub-GPa range, positioning it well below PLLA but above highly compliant soft polymers, and firmly within a low-modulus domain associated with next-generation flexible stent concepts [57].

From a design perspective, the three optimisation pathways delineate distinct material states that map directly onto clinically relevant deployment scenarios. The compression-optimised condition represents a stiffer, higher load-bearing material state suitable for applications where enhanced radial support is required, such as moderately calcified or recoil-prone lesions. In contrast, the flexural-optimised condition corresponds to a more compliant material state, favouring navigation through tortuous or highly curved vessels. The multi-objective solution occupies an intermediate region of the design space, reflecting the practical compromise between radial rigidity and vascular conformability inherent to modern stent design. Crucially, these material states were achieved solely through process-parameter modulation, demonstrating that MEX-fabricated PCL spans a clinically meaningful mechanical spectrum rather than possessing a single intrinsic strength and modulus profile. This tunable material window provides a foundational design space upon which future geometry-driven optimisation strategies may be layered. Therefore, the optimised PCL windows identified in the present study do not function as final stent specifications but as strength and modulus regimes that future stent architectures may selectively leverage depending on the targeted lesion environment. This establishes a direct and clinically grounded link between MEX parameter selection, material-level mechanics and the broader performance envelope required of next-generation BRS.

4.0 Conclusion

This study elucidated the process–structure–property relationships governing the compressive and flexural behaviour of MEX-fabricated PCL, establishing a quantitative, material-level framework relevant to BRS development. Statistical modelling coupled with microstructural observations identified M_E as the primary determinant of mechanical performance, while T_E and v_D acted as secondary modulators of consolidation quality. These findings demonstrate that the mechanical response of MEX-fabricated PCL is governed predominantly by volumetric material delivery rather than thermal or kinematic parameters alone, defining a tunable mechanical window that can be systematically accessed through process optimisation. By decoupling material behaviour from structural geometry, this work provides a robust baseline for future stent-level design and geometry-driven optimisation strategies.

Declarations

Conflict of interests

The authors have no relevant financial or non-financial interests to disclose.

Funding information

This work was funded by the Fundamental Research Grant Scheme (FRGS) under a grant number of FRGS/1/2021/TK0/UNIMAP/02/19 from Ministry of Higher Education Malaysia.

Availability of data and materials

The datasets generated and analysed during the current study are included in this article. Additional data are available from the corresponding author on request.

References

1. Okereke MI, Khalaj R, Tabriz AG, et al (2023) Development of 3D printable bioresorbable drug eluting coronary stents: An experimental and computational investigation. J Drug Deliv Sci Technol 79:103952. https://doi.org/10.1016/j.jddst.2022.103952
2. Wu H, Yang L, Luo R, et al (2024) A drug-free cardiovascular stent functionalized with tailored collagen supports in-situ healing of vascular tissues. Nat Commun 15:735. https://doi.org/10.1038/s41467-024-44902-2
3. Dinc R, Ekingen E (2025) Biodegradable Stents in the Treatment of Arterial Stenosis. J Clin Med 14:532. https://doi.org/10.3390/jcm14020532
4. Xu J, Yang J, Huang N, et al (2016) Mechanical response of cardiovascular stents under vascular dynamic bending. Biomed Eng Online 15:21. https://doi.org/10.1186/s12938-016-0135-8
5. Ahadi F, Azadi M, Biglari M, et al (2023) Evaluation of coronary stents: A review of types, materials, processing techniques, design, and problems. Heliyon 9:e13575. https://doi.org/10.1016/j.heliyon.2023.e13575
6. Pan C, Han Y, Lu J (2021) Structural design of vascular stents: A review. Micromachines (Basel). 12
7. Fang S (2024) Assessing the functional mechanical properties of polycaprolactone stents post-processed by ultrasonic strengthening. J Manuf Process 118:154–162. https://doi.org/10.1016/j.jmapro.2024.03.052
8. Yasmin F, Vafadar A, Tolouei-Rad M (2025) Application of Additive Manufacturing in the Development of Polymeric Bioresorbable Cardiovascular Stents: A Review. Adv Mater Technol 10:. https://doi.org/10.1002/admt.202400210
9. Gallinoro E, Almendarez M, Alvarez-Velasco R, et al (2022) Bioresorbable stents: Is the game over? Int J Cardiol 361:20–28. https://doi.org/10.1016/j.ijcard.2022.05.024
10. Kapoor A, Jepson N, Bressloff NW, et al (2024) The road to the ideal stent: A review of stent design optimisation methods, findings, and opportunities. Mater Des 237:112556. https://doi.org/10.1016/j.matdes.2023.112556
11. Tidwell K, Harriet S, Barot V, et al (2021) Design and Analysis of a Biodegradable Polycaprolactone Flow Diverting Stent for Brain Aneurysms. Bioengineering 8:183. https://doi.org/10.3390/bioengineering8110183
12. Sousa AM, Amaro AM, Piedade AP (2022) 3D Printing of Polymeric Bioresorbable Stents: A Strategy to Improve Both Cellular Compatibility and Mechanical Properties. Polymers (Basel) 2022:1099. https://doi.org/10.3390/polym

13. Zhao J, Song G, Zhao Q, et al (2023) Development of three-dimensionally printed vascular stents of bioresorbable poly(l-lactide-co-caprolactone). J Biomed Mater Res B Appl Biomater 111:656–664. https://doi.org/10.1002/jbm.b.35184
14. Jeong Y-J, Choi B, Kim S, et al (2024) Fully bioresorbable, all-polymer-based, 3D-printed scaffolds with prolonged radiopacity and enhanced durability. Chemical Engineering Journal 494:152851. https://doi.org/10.1016/j.cej.2024.152851
15. Szymczyk-Ziółkowska P, Łabowska MB, Detyna J, et al (2020) A review of fabrication polymer scaffolds for biomedical applications using additive manufacturing techniques. Biocybern. Biomed. Eng. 40:624–638
16. Jiang W, Zhao W, Zhou T, et al (2022) A Review on Manufacturing and Post-Processing Technology of Vascular Stents. Micromachines (Basel). 13
17. Li Y, Shi Y, Lu Y, et al (2023) Additive manufacturing of vascular stents. Acta Biomater. 167:16–37
18. Patel R, Jani S, Joshi A (2023) Review on multi-objective optimization of FDM process parameters for composite materials. International Journal on Interactive Design and Manufacturing (IJIDeM) 17:2115–2125. https://doi.org/10.1007/s12008-022-01111-9
19. Guerra AJ, Ciurana J (2018) 3D-printed bioabsordable polycaprolactone stent: The effect of process parameters on its physical features. Mater Des 137:430–437. https://doi.org/10.1016/j.matdes.2017.10.045
20. Wang C, Zhang L, Fang Y, Sun W (2021) Design, Characterization, and 3D Printing of Cardiovascular Stents with Zero Poisson's Ratio in Longitudinal Deformation. Engineering 7:979–990. https://doi.org/10.1016/j.eng.2020.02.013
21. Singh J, Singh G, Pandey PM (2021) Multi-objective optimization of solvent cast 3D printing process parameters for fabrication of biodegradable composite stents. International Journal of Advanced Manufacturing Technology 115:3945–3964. https://doi.org/10.1007/s00170-021-07423-6
22. Kandi R, Pandey PM (2021) Statistical modelling and optimization of print quality and mechanical properties of customized tubular scaffolds fabricated using solvent-based extrusion 3D printing process. Proc Inst Mech Eng H 235:1421–1438. https://doi.org/10.1177/09544119211032012
23. Brunelli M, Perrault CM, Lacroix D (2017) Mechanical response of 3D Insert® PCL to compression. J Mech Behav Biomed Mater 65:478–489. https://doi.org/10.1016/j.jmbbm.2016.08.038
24. Wang Q, Fang G, Zhao Y-H, Zhou J (2018) Improvement of Mechanical Performance of Bioresorbable Magnesium Alloy Coronary Artery Stents through Stent Pattern Redesign. Applied Sciences 8:2461. https://doi.org/10.3390/app8122461
25. Wei Y, Wang M, Zhao D, et al (2019) Structural Design of Mechanical Property for Biodegradable Polymeric Stent. Advances in Materials Science and Engineering 2019:1–14. https://doi.org/10.1155/2019/2960435
26. Samant S, Wu W, Zhao S, et al (2021) Computational and experimental mechanical performance of a new everolimus-eluting stent purpose-built for left main interventions. Sci Rep 11:8728. https://doi.org/10.1038/s41598-021-87908-2

27. Wang Y, Wu H, Fan S, et al (2023) Structure design and mechanical performance analysis of three kinds of bioresorbable poly-lactic acid (PLA) stents. Comput Methods Biomech Biomed Engin 26:25–37. https://doi.org/10.1080/10255842.2022.2045485
28. Carbonaro D, Ferro N, Mezzadri F, et al (2024) Easy-to-use formulations based on the homogenization theory for vascular stent design and mechanical characterization. Comput Methods Programs Biomed 257:108467. https://doi.org/10.1016/j.cmpb.2024.108467
29. Wang L, Jiao L, Pang S, et al (2021) The development of design and manufacture techniques for bioresorbable coronary artery stents. Micromachines (Basel) 12:. https://doi.org/10.3390/mi12080990
30. Bai C, Feng X, Lan L, et al (2025) Recent advances and perspectives in bioresorbable metal coronary drug-eluting stents. Biomedical Materials 20:032001. https://doi.org/10.1088/1748-605X/adc058
31. Eshraghi S, Das S (2010) Mechanical and microstructural properties of polycaprolactone scaffolds with one-dimensional, two-dimensional, and three-dimensional orthogonally oriented porous architectures produced by selective laser sintering. Acta Biomater 6:2467–2476. https://doi.org/10.1016/j.actbio.2010.02.002
32. Eshraghi S, Das S (2012) Micromechanical finite-element modeling and experimental characterization of the compressive mechanical properties of polycaprolactone–hydroxyapatite composite scaffolds prepared by selective laser sintering for bone tissue engineering. Acta Biomater 8:3138–3143. https://doi.org/10.1016/j.actbio.2012.04.022
33. Alemán-Domínguez ME, Giusto E, Ortega Z, et al (2019) Three-dimensional printed polycaprolactone-microcrystalline cellulose scaffolds. J Biomed Mater Res B Appl Biomater 107:521–528. https://doi.org/10.1002/jbm.b.34142
34. Wang S, Ma Y, Deng Z, et al (2020) Effects of fused deposition modeling process parameters on tensile, dynamic mechanical properties of 3D printed polylactic acid materials. Polym Test 86:106483. https://doi.org/10.1016/j.polymertesting.2020.106483
35. Hsueh M-H, Lai C-J, Wang S-H, et al (2021) Effect of Printing Parameters on the Thermal and Mechanical Properties of 3D-Printed PLA and PETG, Using Fused Deposition Modeling. Polymers (Basel) 13:1758. https://doi.org/10.3390/polym13111758
36. Kamaal M, Anas M, Rastogi H, et al (2021) Effect of FDM process parameters on mechanical properties of 3D-printed carbon fibre–PLA composite. Progress in Additive Manufacturing 6:63–69. https://doi.org/10.1007/s40964-020-00145-3
37. Al-Tamimi AA, Pandžić A, Kadrić E (2023) Investigation and Prediction of Tensile, Flexural, and Compressive Properties of Tough PLA Material Using Definitive Screening Design. Polymers (Basel) 15:4169. https://doi.org/10.3390/polym15204169
38. Valvez S, Silva AP, Reis PNB (2022) Optimization of Printing Parameters to Maximize the Mechanical Properties of 3D-Printed PETG-Based Parts. Polymers (Basel) 14:2564. https://doi.org/10.3390/polym14132564

39. He S, Chen Q, Li Z (2025) Influence of Stent Structure on Mechanical and Degradation Properties of Poly (Lactic Acid) Vascular Stent. J Funct Biomater 16:248. https://doi.org/10.3390/jfb16070248
40. Noad RL, Hanratty CG, Walsh SJ (2011) Clinical Impact of Stent Design. Interventional Cardiology Review 9:89. https://doi.org/10.15420/icr.2011.9.2.89
41. Park J, Kwak HS, Kim J-W (2020) Bench-Top Comparison of Three Different Types of Stents Used for Treatment of Intracranial Atherosclerotic Stenosis. Neurointervention 15:117–125. https://doi.org/10.5469/neuroint.2020.00248
42. Ang HY, Huang YY, Lim ST, et al (2017) Mechanical behavior of polymer-based vs. metallic-based bioresorbable stents. J Thorac Dis 9:S923–S934. https://doi.org/10.21037/jtd.2017.06.30
43. Gautam AJ, Wairkar S (2024) 3D-printed bioresorbable vascular stents: emerging frontiers in personalized cardiac care. Polymer Bulletin 81:10533–10560. https://doi.org/10.1007/s00289-024-05237-6
44. Tang C, Liu J, Yang Y, et al (2020) Effect of process parameters on mechanical properties of 3D printed PLA lattice structures. Composites Part C: Open Access 3:. https://doi.org/10.1016/j.jcomc.2020.100076
45. Wang P, Zou B, Ding S, et al (2021) Effects of FDM-3D printing parameters on mechanical properties and microstructure of CF/PEEK and GF/PEEK. Chinese Journal of Aeronautics 34:236–246. https://doi.org/10.1016/j.cja.2020.05.040
46. Fernandez-Vicente M, Calle W, Ferrandiz S, Conejero A (2016) Effect of Infill Parameters on Tensile Mechanical Behavior in Desktop 3D Printing. 3D Print Addit Manuf 3:183–192. https://doi.org/10.1089/3dp.2015.0036
47. Samykano M, Selvamani SK, Kadirgama K, et al (2019) Mechanical property of FDM printed ABS: influence of printing parameters. The International Journal of Advanced Manufacturing Technology 102:2779–2796. https://doi.org/10.1007/s00170-019-03313-0
48. Sagar A, Nehme C, Saigal A, James TP (2020) Stress–Strain Relationship of Polycaprolactone in Liquid Nitrogen for Finite Element Simulation of Cryogenic Micropunching Process. J Eng Sci Med Diagn Ther 3:. https://doi.org/10.1115/1.4047461
49. Abdul Haq RH, Saidin W, Mat UW (2013) Improvement of Mechanical Properties of Polycaprolactone (PCL) by Addition of Nano-Montmorillonite (MMT) and Hydroxyapatite (HA). Applied Mechanics and Materials 315:815–819. https://doi.org/10.4028/www.scientific.net/AMM.315.815
50. Jiao Z, Luo B, Xiang S, et al (2019) 3D printing of HA / PCL composite tissue engineering scaffolds. Advanced Industrial and Engineering Polymer Research 2:196–202. https://doi.org/10.1016/j.aiepr.2019.09.003
51. Siqueira DD, Luna CBB, Araújo EM, et al (2019) Biocomposites based on PCL and macaiba fiber. Detailed characterization of main properties. Mater Res Express 6:095335. https://doi.org/10.1088/2053-1591/ab3496
52. Abbas A, Park EJ, Guo J, et al (2024) Performance of bioresorbable peptide incorporated polymers produced for fused deposition modelling (FDM). Next Materials 5:100223.

https://doi.org/10.1016/j.nxmate.2024.100223

53. Toorani S, Sohrabian M, Sameezadeh M, Khalafi M (2025) Optimized Fabrication and Enhanced Flexural Properties of PCL/F-BG Nanocomposites for Hard Tissue Engineering. J Polym Environ 33:5130–5148. https://doi.org/10.1007/s10924-025-03710-5
54. Brand M, Sharon N (2025) Analytical Modeling and Validation of Radial Stiffness in Zigzag-Shaped Stents: Experimental and Numerical Approaches. J Biomed Mater Res B Appl Biomater 113:. https://doi.org/10.1002/jbm.b.35574
55. Katagiri Y, Stone G, Onuma Y, Serruys P (2017) State of the art: the inception, advent and future of fully bioresorbable scaffolds. EuroIntervention 13:734–750. https://doi.org/10.4244/EIJ-D-17-00499
56. Farhan M, Hasan G, Sobhi A, et al (2025) Bioresorbable scaffolds advances, challenges, and future directions. Annals of Medicine & Surgery 87:4173–4183. https://doi.org/10.1097/MS9.0000000000003424
57. Xu D, Harvey T, Begiristain E, et al (2022) Measuring the elastic modulus of soft biomaterials using nanoindentation. J Mech Behav Biomed Mater 133:105329. https://doi.org/10.1016/j.jmbbm.2022.105329

Figures

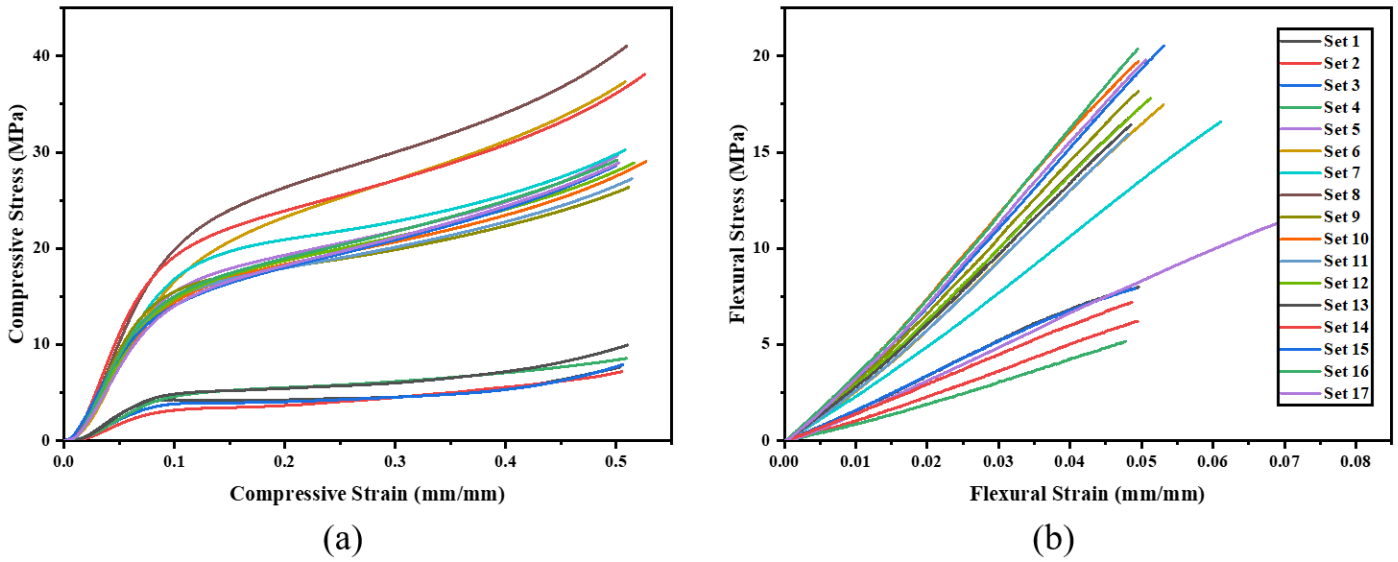


Figure 1

Representative stress–strain responses of MEX-fabricated PCL specimens under (a) compression and (b) flexure. Each curve corresponds to a distinct process parameter set (Set 1–Set 17) generated using the CCD-based response surface design.

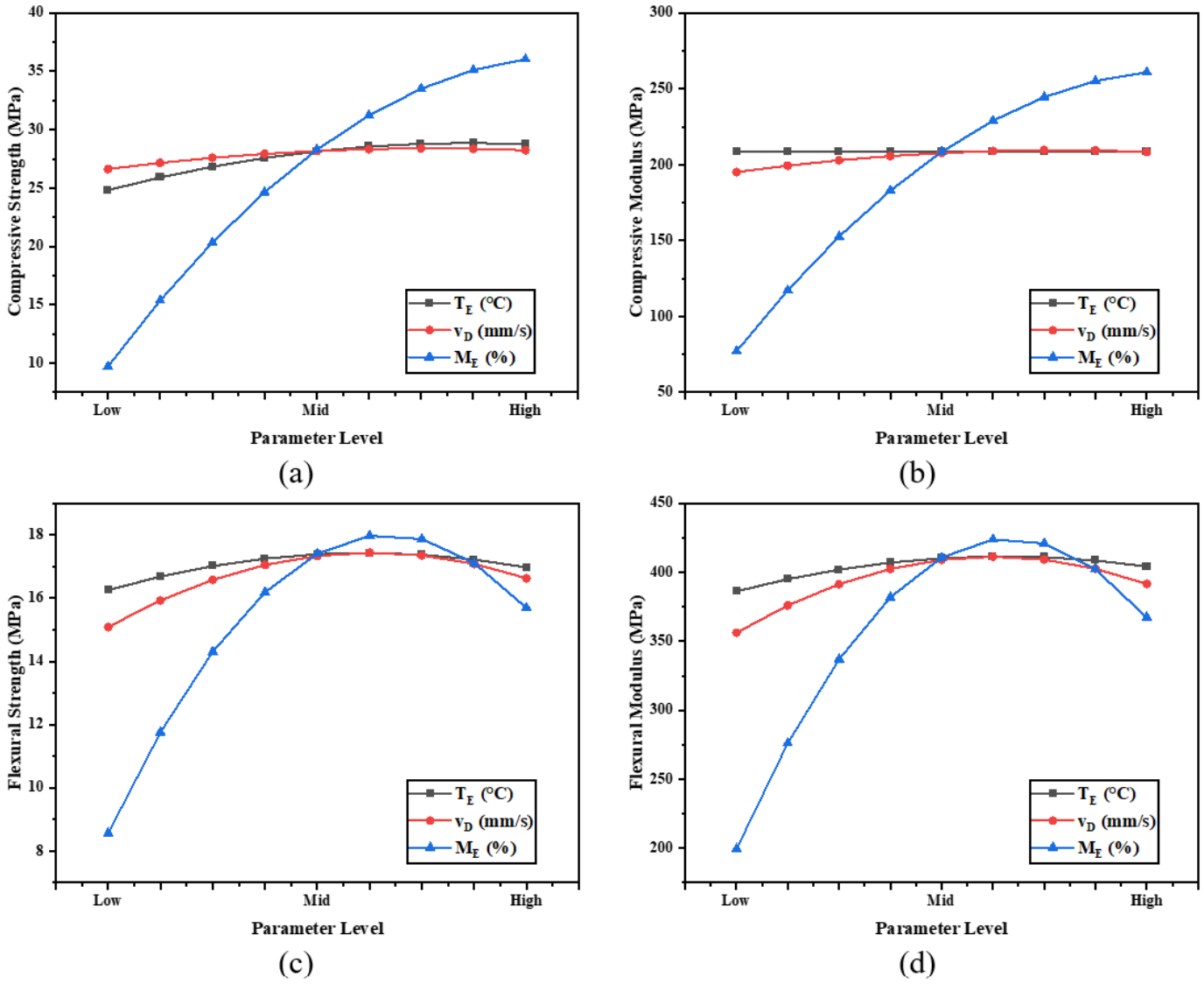


Figure 2

Main effect plots of T_E, v_D and M_E on (a) compressive strength, (b) compressive modulus, (c) flexural strength and (d) flexural modulus.

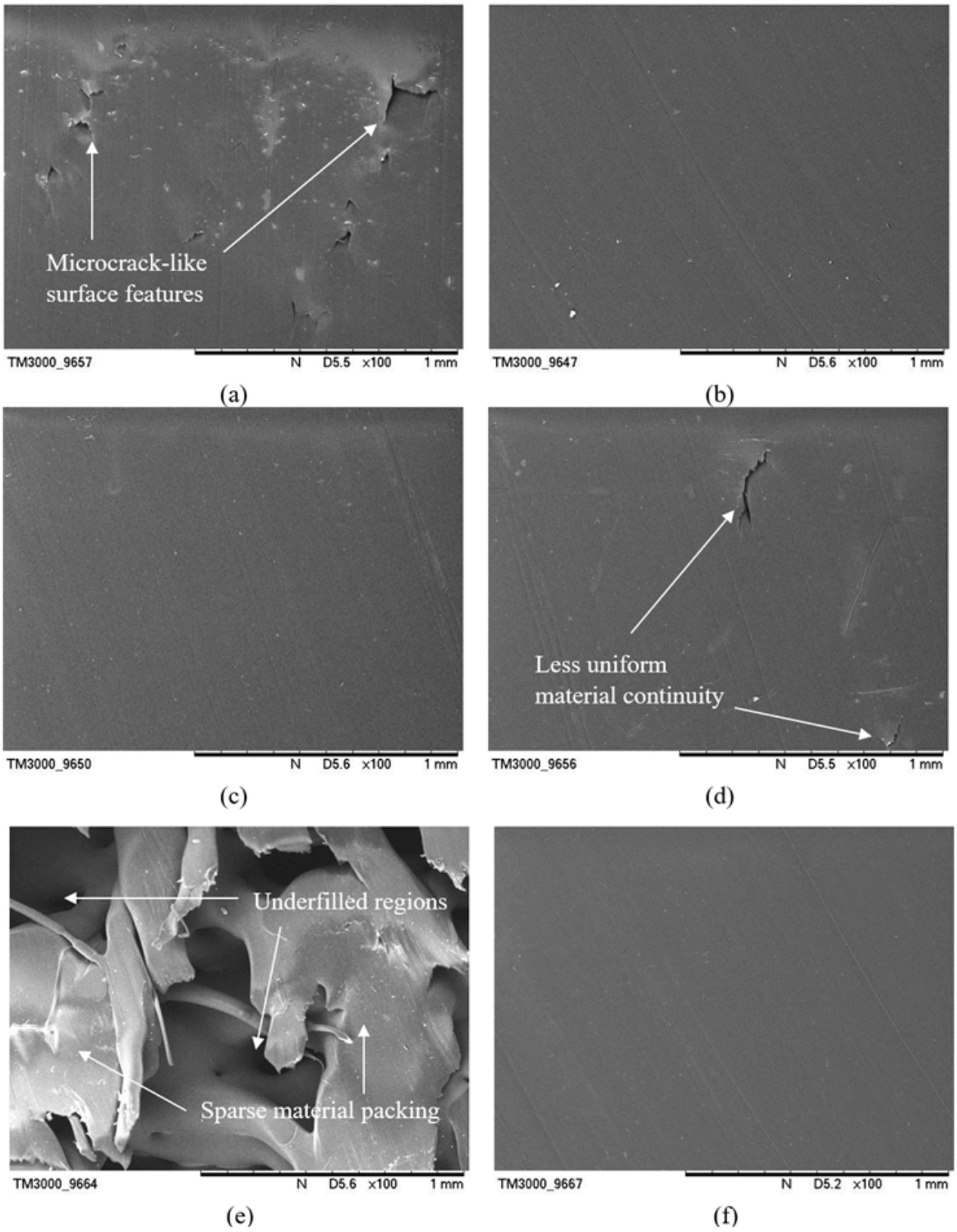


Figure 3

Representative cross-sectional SEM micrographs of MEX-fabricated PCL specimens for compression testing acquired at 100× magnification, illustrating the effects of extreme process parameters on consolidation-related morphology. (a) Low T_E (80 °C); (b) high T_E (250 °C); (c) low v_D (5 mm/s); (d) high v_D (50 mm/s); (e) low M_E (70%); and (f) high M_E (150%).

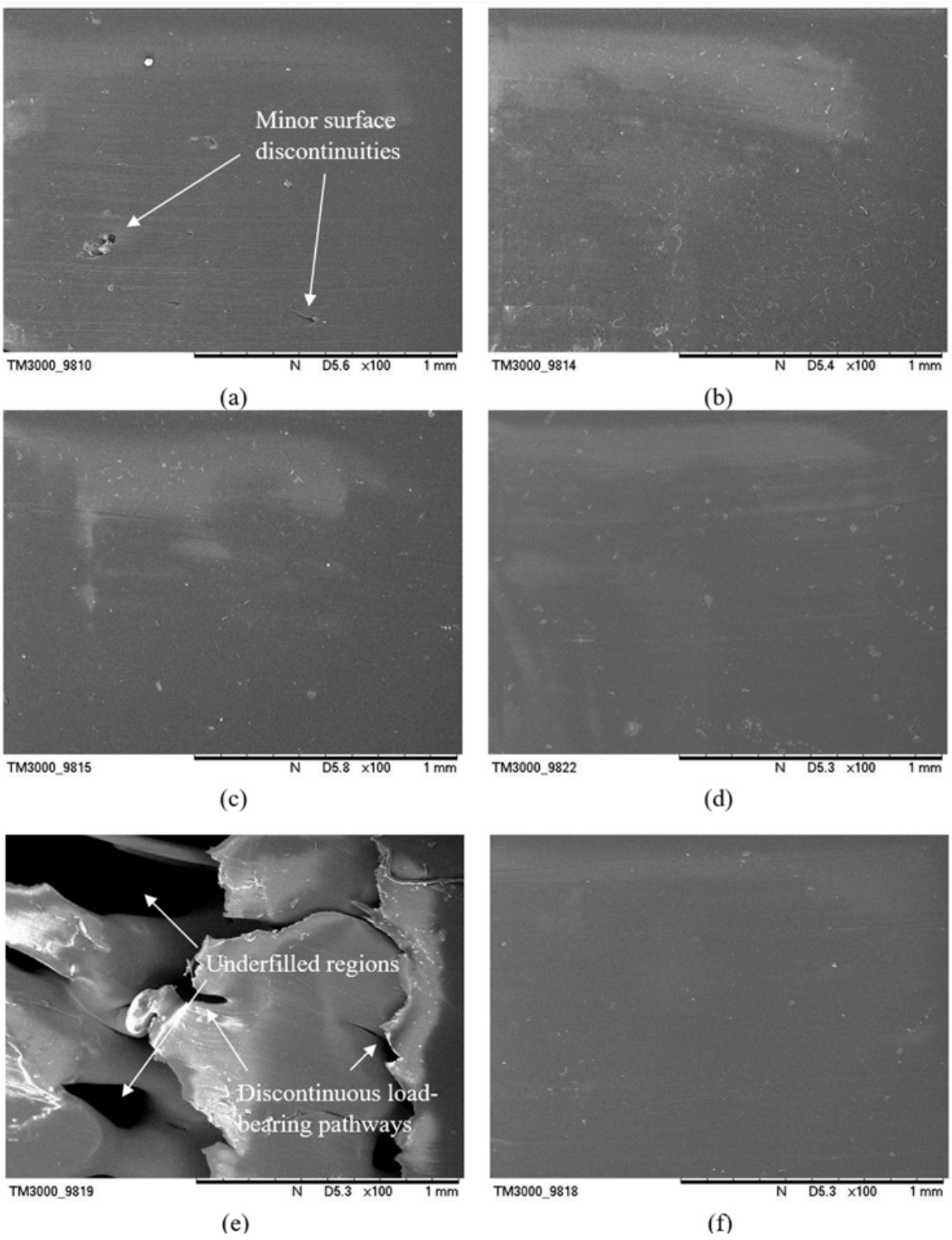


Figure 4

Representative cross-sectional SEM micrographs of MEX-fabricated PCL specimens for flexural testing acquired at 100× magnification, illustrating the effects of extreme process parameters on consolidation-related morphology. (a) Low T_E (80 °C); (b) high T_E (250 °C); (c) low v_D (5 mm/s); (d) high v_D (50 mm/s); (e) low M_E (70%); and (f) high M_E (150%).

Supplementary Files

This is a list of supplementary files associated with this preprint. Click to download.

- GraphicalAbstract.pdf